Boehmite agglomeration through experimental and model approaches : from colloidal system to porous solid

Giulia Ferri, Severine Humbert, Mathieu Digne, Maxime Moreaud, Jean-Marc Schweitzer

Boehmite agglomeration through experimental and model approaches : from colloidal system to porous solid

Giulia Ferri[a,1], Severine Humbert[a], Mathieu Digne[a], Maxime Moreaud[a,b], Jean-Marc Schweitzer[a]

[a] *IFP Energies nouvelles, Rond-point de l'changeur de Solaize, 69360 Solaize, France.*
[b] *CMM MINES ParisTech, PSL-Research University, Fontainebleau, 77305 Seine-et-Marne, France*

Abstract

The agglomeration dynamics within colloidal boehmite suspensions is crucial to understand the formation of a porous boehmite network during the manufacturing of γ-alumina catalyst carriers. Such carriers are frequently used in petroleum hydrotreating processes and must have specific textural characteristics. The method described in this work enables to model the three-dimensional morphology of colloidal agglomerates of boehmite for different conditions of pH in the colloidal mixture. These agglomerates are then used to generate a boehmite grain, whose textural properties can be numerically estimated. The coagulation kinetics has been studied with experimental Dynamic Light Scattering and Lagrangian model including Brownian dynamics and DLVO interaction potential. The adjustment of the Brownian aggregation kernel of a population-balance model enables to estimate the agglomerates size distribution and fractal dimension.

Keywords: Colloidal agglomeration, Fractal dimension, Catalyst carrier.

1. Introduction

Tuning the porosity of catalytic supports is attracting significant interest for the control of reaction kinetics in many industrial processes. Most of the used catalytic supports are in γ-alumina, prepared from boehmite powder which undergoes several processing steps where its water content varies. Boehmite (the γ-alumina precursor) passes from the powder, to the paste and finally to the porous solid state. During these processes, structural changes occur at the meso- and macro-scale, which have an impact on the final porosity of the solid and its performance as a catalytic support. The structure of γ-alumina catalyst carrier is due to the organisation of primary boehmite crystallites, of a few nm [1], formed during a precipitation phase. The primary crystallites assemble to form aggregates and agglomerates. The shape of crystallites, aggregates and agglomerates determines the type of porosity at micro-, meso- and macro-scale [2].

In order to perform a tailored synthesis of γ-alumina supports in the coming years, it is necessary to develop an experimental and numerical method to study the effect that the operating conditions of the manufacturing process have on the structure of a porous solid. In this study we focus on the effect that the chemical composition of a colloidal suspension of boehmite has on the fractal dimension and on the size distribution of boehmite agglomerates. Our strategy (see Fig.1) enables to describe the morphology of the solid structure according to synthesis parameters. To this purpose, ideal and low concentration boehmite suspension have been studied under Brownian conditions. In these conditions, we are in an ideal case where the physical interactions are fully theorized. Therefore, no unknown parameters are used to fit the experimental data set. These systems have been described using theoretical models of colloidal agglomeration (like DLVO theory [3, 4] and Smoluchowski equation [5]).

The experimental characterisation of coagulating colloidal suspension via DLS (dynamic light scattering) provides data for the adjustment of the aggregation kernels of a population-balance model.

A discrete-element model, relying on DLVO and

[1] Present address: Politecnico di Milano, Dipartimento di Energia, Via La Masa 34, 20156, Milano; Italy
Corresponding author: giulia.ferri@polimi.it

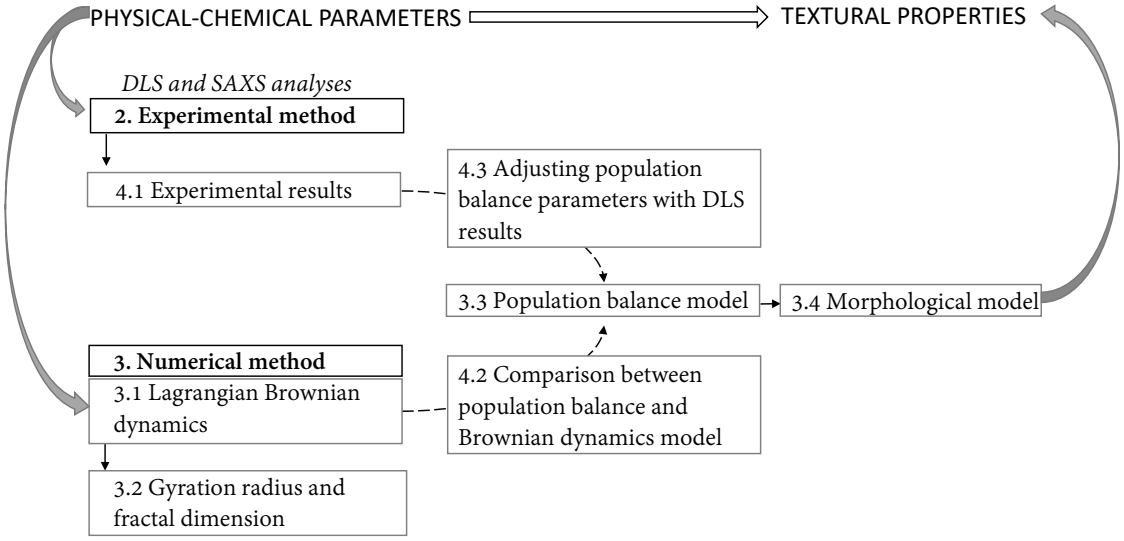

Figure 1: Strategy to estimate textural properties of a boehmite porous solid according to the physical-chemical parameters of Brownian agglomeration.

Langevin [6] theories, enables to fill the experimental gaps and to estimate the evolution of average radius and fractal dimension along the agglomeration process. The fractal dimension d_f is here considered as a structural parameter to characterise individual agglomerates. The Lagrangian approach and the population balance can represent agglomeration under Brownian motion and a validation is possible between these two modeling approaches. These models both depend on the Fuchs stability coefficient, which is a function of the pH and ionic strength of the colloidal suspension. The Fuchs stability ratio reaches a value close to unity for strongly unstable suspensions which have a high tendency to agglomerate [7], its theoretical value can be computed from the DLVO interaction potential U^{tot}

$$W \approx \frac{1}{2\kappa a} exp\left(\frac{U^{tot,max}}{k_B T}\right) \quad (1)$$

assuming spherical particles of radius a, homogeneous surface charge distribution and negligible solvation force. r is the distance between the centers of the two particles, k_B is the Boltzmann constant and T is the temperature.

$$\kappa = \left(\frac{\epsilon k_B T}{2e^2 A_v}\right)^{-0.5} \sqrt{I} \quad (2)$$

is the inverse of the Debye length, the length of the layer of ions that are strongly bond to the particles and screen the electrical field of the particle.

The Lagrangian model input parameters are the size of the primary particles, the boehmite concentration and W. The model results is a dependence of the fractal dimension on the gyration radius. This dependence justifies the consideration of a size-dependent fractal dimension and is an input of the population balance, where the Smoluchowski kernel is considered. The population balance also depends on the size distribution of the primary dispersed boehmite particles (in our case a Dirac function), on W and on the boehmite concentration. The result of the population balance is the size distribution of the boehmite agglomerates at the end of the agglomeration process.

The relationship between the fractal dimension and the agglomerate gyration radius, and the agglomerate size distribution are th input parameters of a morphological agglomeration model [8], whose result is the final morphology an agglomerates assembly. This last model is based on a random sequential addition algorithm and on morphological operators. It does not describe the coagulation physics, but simulates a stochastic assembly of particles. It is suitable for the simulation of a realistically large morphology, which makes possible the estimation of textural properties.

2. Experimental methods

Boehmite suspensions were prepared using a highly dispersible powder (Pural SB3, from Sasol GmbH) with a loss on ignition of 26%. The suspension was prepared with a concentration of boehmite powder of 0.04 g/L. The boehmite concentration was chosen according to the measurement techniques. Indeed, the coagulation time scale must be of the same order of magnitude of the acquisition time. The nitric acid (1M Fisher Scientific J/5550/PB15) concentration has been chosen in order to peptize the boehmite powder at a pH around 3, 0.0015 M. In order to control the pH, ammonia has been injected (1M Chem-Lab CL05.0101.1000). The pH was measured using a pH-meter (Seven2Go Mettler Toledo). The zeta potential measurement have been performed with Malvern Zetasizer Nano ZS with 1 mL sample using capillary cells with electrodes. A study of the titration curve and the corresponding zeta potential vs pH curves was realized to tune the zeta potential via NH_3 injection in the initial peptized boehmite suspension.

DLS measurement were performed with Malvern Zetasizer Nano ZS, using square polysyrene cell. 1 mL of initial peptized suspension was taken, filtered with a syringe filter at 5 μm. This procedure was necessary to remove any dust that could falsify the measurement and to eliminate the few grains of un-peptized powder that would not be visible with DLS. The initial suspension is characterized. Then, 0.2 ml of ammonia (and/or NaCl) solution was injected in the measurement cell and the in-situ analysis was started. The average diameter was computed with the cumulant method [9].

SAXS analyses were performed at the SWING beamline of SOLEIL synchrotron in Saint Aubin, France. The incident energy of the X-ray beam was 10 keV. 200 mL of the initial suspension were placed in a stirred reactor, the sample was pumped continuously through a quartz capillary of 1.5 mm. The injection of 40 ml of the ammonia was achieved via remote control of two syringes. The average gyration radius and fractal dimension was computed using the Beaucage model [10].

3. Numerical methods

Three numerical approaches were used to model the colloidal agglomeration process and the morphology of the agglomerates. Concerning the agglomeration process, the two methods were Brownian dynamics and the population balance equation. The first enabled to simulate fast agglomeration kinetics, which cannot be observed experimentally, giving insight into the evolution of the size and fractal dimension of agglomerates in a system under Brownian conditions and according to the DLVO interaction potential. The drawback was, however, the computation time, which became very high for the simulation of large systems. The second, the population balance, enabled to simulate the evolution of a system consisting of a large number of particles. The third approach allowed to build the morphology of colloidal agglomerates using stochastic packings of elementary objects.

3.1. Lagrangian Brownian dynamics

The Lagrangian model was described in a previous work [8]. The initial system was composed by 2048 identical spherical particles of radius a =40 nm, with homogeneous surface charge within a cube of length 3800 nm. A random sequential addition algorithm was used to generate the initial positions of the spheres using particle a concentration of 1%. The dynamics of each sphere i was computed via the momentum balance

$$m_i \cdot \vec{a_i} = \sum_{i \neq j} \vec{F_{ij}} + \vec{F_i^R} + \vec{F_i^D}, \tag{3}$$

where m_i and a_i are the mass and the acceleration of the particle. $\vec{F_{ij}}$ is the DLVO interaction force deriving from DLVO potential [3], the model accounts for the interaction between the particle i and all the other particles j contained within an interaction sphere of radius $6a$. Indeed, the interaction forces between particles at a larger distance are negligible. This leads to a significant reduction in calculation time.

$\vec{F_i^R}$ is the random Langevin force (accounting for Brownian motion)

$$\vec{F_i^R} = \sqrt{2 \cdot k_B \cdot T} \cdot \vec{W} \tag{4}$$

where $\vec{W}$ is a random vector whose components are independent Gaussian random numbers with zero mean and unit variance.

$\vec{F_i^D}$ is the viscous drag force (Stoke's law)

$$\vec{F_i^D} = -6 \cdot \pi \cdot \mu \cdot a \cdot \vec{v_i} \tag{5}$$

which depends on the viscosity of the medium μ, on the velocity of the particle $\vec{v_i}$ and on the particle radius a.

A semi-implicit finite differences method was used for numerical integration [11]. In order to ensure robustness when the particles are close to each other (the DLVO potential tends to - infinity when the particles are in contact), a contact force was added when two particles were at a distance lower than $2a$ which was modeled as a Hertz contact force [12]. In order to approach the behaviour of an infinite medium, periodic boundary conditions were implemented [13]. Identical spheres of 40 nm radius were considered within a cubic volume of 3800 nm side. The volume fraction occupied by the spheres is 1 %, leading to 2048 spheres. At time 0, a minimum interparticle distance of 1 nm is imposed. An ionic strength of 0.005 M and a surface potential of 1 mV, which is characteristic of conditions close to the point of zero charge, are considered.

3.2. Gyration radius and fractal dimension

When the positions of all the spheres at a given time instant are known, it is possible to compute the gyration radius R_{gyr} and the fractal dimension d_f of the agglomerates [14]

$$d_f = \frac{\log\left(\frac{\xi}{k_f}\right)}{\log\left(\frac{R_{gyr}}{R}\right)}, \tag{6}$$

where ξ is the number of primary particles (spheres of 40 nm radius) that constitute the aggregate and k_f is the fractal pre-factor [15] fixed at 1.2 [8].

R_{gyr} is given by the geometrical average distance between the spheres'centers and the agglomerate center of mass. The formula used by Filippov *et al.*[16] contains also the radius of the primary particle a, so that for $\xi \to 1$, $R_{gyr} \to a$:

$$R_{gyr}^2 = \frac{1}{\xi}\sum_{i=1}^{\xi}\Big[(x_i - x_g)^2 + (y_i - y_g)^2 + \\ + (z_i - z_g)^2 + a^2\Big] \tag{7}$$

where the coordinates of the centers of the spheres are x_i, y_i and z_i and the coordinates of the agglomerate center of mass are x_g, y_g and z_g:

$$x_g = \frac{\sum_i^{\xi} x_i}{\xi}; \tag{8}$$

$$y_g = \frac{\sum_i^{\xi} y_i}{\xi}; \tag{9}$$

$$z_g = \frac{\sum_i^{\xi} z_i}{\xi}. \tag{10}$$

3.3. The population balance model

The population balance equation was used to describe the evolution of large colloidal boehmite systems in terms of size distribution and number of primary particles 10^{21}. The governing equation was solved in its discrete form

$$\frac{dN_k}{dt} = \frac{1}{2}\sum_{i=1}^{k-1}\beta_{i,k-i}^{agg} N_i N_{k-i} - N_k \sum_{i=1}^{\infty}\beta_{ik}^{agg} N_i \tag{11}$$

where

- N_k is the concentration number of clusters of mass ξ_k, where the mass means the number of primary particles constituing the aggregate k;
- the first term represents all possible collisions leading to the formation of an aggregate of mass ξ_k;
- the second term represents the rate of disappearance of the aggregates of mass ξ_k due to aggregation with aggregates of any mass;
- the β terms are Brownian agglomeration kernels

$$\beta_{i,j} = \frac{2}{3}\frac{k_B T}{\eta W}(\xi_i^{1/d_f} + \xi_j^{1/d_f})\left(\xi_i^{-1/d_f} - \xi_j^{-1/d_f}\right); \tag{12}$$

The number of primary particles in each agglomerate was related to the agglomerate fractal dimension via the relationship in Eq.(6).

The population balance parameters that were adjusted with DLS data are the Fuchs coefficient W and the parameters of the curve $d_f = f(R_{gyr})$. For this latter, an arctangent function was used to reproduce the shape obtained from the Lagrangian simulation. However, the parameters of this function were adjusted with experimental data, because Lagrangian simulation is impacted by the low number of particles and by the assumption of periodic conditions involving agglomerates breakage.

Before adjusting the model kernels with DLS data, it was necessary to consider the maximum radius that could be measured with DLS as well as the type of weighting to compute the average agglomerate radius. Indeed it was necessary to "cut" the population distribution to a maximum agglomerate radius R_{gyr}^{lim} of 1.5 μm. This entailed a limit mass number of

$$\xi^{lim} = k_f \cdot \left(\frac{R_{gyr}^{lim}}{a}\right)^{d_f} \tag{13}$$

where k_f is the fractal pre-factor (assumed equal to 1.2 [17]) and a is the radius of the primary particle. The cut population is composed by all the agglomerates that have

$$\xi \leq \xi^{lim}. \tag{14}$$

Afterwards it was necessary to estimate a weighted average radius considering that DLS measures an effective diffusion coefficient based on how quickly the intensity of the scattered light changes. The diffusion coefficient is then related to the average radius R via the Stokes-Einstein law

$$D = \frac{k_B \cdot T}{6\pi \cdot \mu \cdot R}. \tag{15}$$

Considering the effective scattering coefficient described by [18]

$$D_{eff} \simeq \frac{\int_0^\infty R_i^6 \cdot D_i \cdot G_i \cdot dR}{\int_0^\infty R_i^6 \cdot G_i \cdot dR}, \tag{16}$$

where D_{eff} is the effective diffusion coefficient, R_i, D_i and G_i are the radius, the diffusion coefficient and the number distribution of particles within the class i. By substituting D_i with the Stokes-Einstein law. Eq.(16) in a discretized form becomes

$$D_{eff} \simeq \frac{\sum_{i=1}^{n_{class}} R_i^6 \cdot D_i \cdot N_{p,i}}{\sum R_i^6 \cdot N_{p,i}}. \tag{17}$$

According to the Stokes-Einstein law the average radius $\bar{R}$ is related to the effective diffusion coefficient

$$\bar{R} \simeq \frac{\frac{6\pi \cdot \mu}{k_B \cdot T}}{D_{eff}}. \tag{18}$$

Substituting Eq.(17) in Eq.(18) leads to

$$\bar{R} \simeq \frac{\sum_{i=1}^{n_{class}} R_i^6 \cdot N_{p,i}}{\sum_{i=1}^{n_{class}} R_i^5 \cdot N_{p,i}} \tag{19}$$

which is the average weighted radius consistent with the DLS principle. The algorithm of Levenberg-Marquardt was used to adjust W and the parameters of the $d_f = f(R_{gyr})$ relationship.

3.4. Morphological model

The morphological aggregation model [8] relies on a sequential aggregation of primary objects. It enables to tune the compactness of the final assemblies according to the probability of sticking the primary objects ether in the concave points or in concave points close to the center of mass of the assembly. In the case of identical spherical primary objects, a specific numerical scheme enables to build assemblies of several millions of primary objects. In order to build the agglomerates within the size range predicted by the population balance, a resolution of 35 nm^2/voxel was considered. A discretized agglomerates mass distribution was built from the solution of the population balance equation. The agglomerates belonging to such distribution were used as primary agglomerates to build an agglomerate of agglomerates, respecting the distribution [19].

4. Results

4.1. Experimental results

The evolution of the average gyration radius measured with DLS i reported, for different pH, in Fig.2(a). These results are qualitatively in agreement with DLVO theory [3] since the closer the pH is to the PZC, the more unstable the suspension, and therefore the more favoured is the agglomeration.

In Fig.2(b) we find the value of Fuchs W using the theoretical formula in Eq.(1) and the experimental values computed according to Holthoff *at al.* [20] (details on the computation are in Appendix A).

The DLS results for pH within the range 8.8 - 9.7 are similar, leading to a quite fast growth of the average hydrodynamic radius. Indeed these conditions are close to the point of zero change (PZC) of the boehmite which is at pH 9 [21]. At pH 10.5 and at pH 11 the agglomeration is slower but still visible within 20 minutes.

For a pH within 8.8 and 10.5, all the experimental points show an initial rapid growth, followed by a slower one. The high variability of the mean radius can be due to several factors. First, the low boehmite concentration, necessary to observe slow kinetics, decreases the signal-to-noise ratio. In addition, the necessity of maintaining Brownian conditions imposed that the suspensions were not mixed after the ammonia injection, leading to polydisperse systems. The experiments at pH 11 show different linear behaviour on Fig.2(a), this can be attributed to the fact that local pH variations have a strong influence on the agglomeration in the first few seconds and then, as the suspension evolves slowly, there is less noise.

Additional information can be extracted from the results of the SAXS analysis, where the scattering curves were interpreted with the Beaucage model using the method adopted by Speyer *et al.* [22].

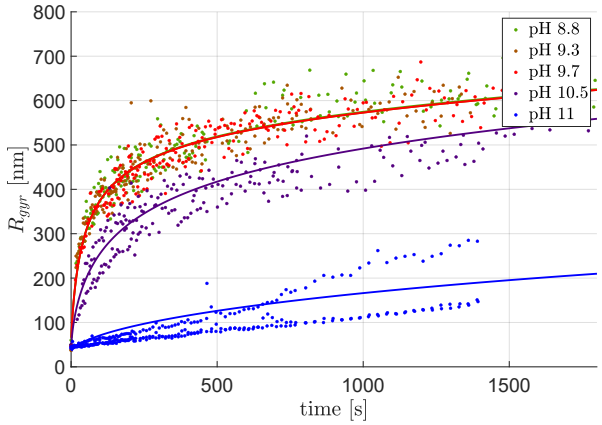

(a)

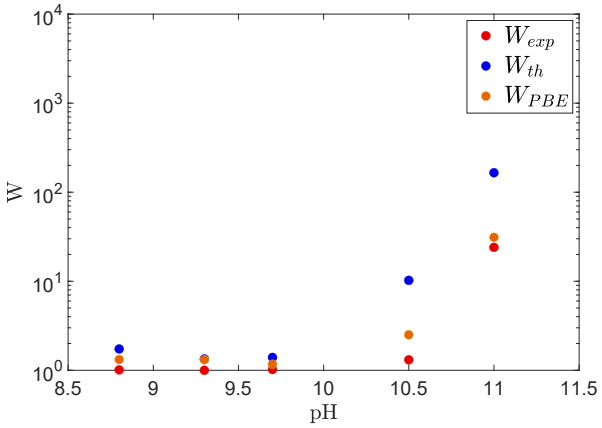

(b)

Figure 2: (a)Evolution of average hydrodynamic intensity radius, measured with DLS on a Pural SB3 suspension of 0.04 g/L and different pH. Comparison between experimental results (dots) and the adjusted population balance model (lines). (b)Fuchs stability ratio: comparison between theoretical [3], experimental[20] and the population balance value.

These analyses offer insight about the fractal dimension of the agglomerates, and how it changes with gyration radius, as can be seen in Fig.3.

These results are related to the size limits of the analysis and the approach used for the interpretation of the SAXS curves. In this regard, it is to be noted that our results refer to agglomerates whose gyration radius is between 50 and 150 nm.

A quasi-linear trend can be observed in the phase diagram. This result enables us to assume that the fractal dimension changes as a function of agglomeration size. In the bottom right plot, it can be observed that for pH 8 and 9.5 (near the point of Zero Charge) the fractal size has a fairly rapid initial growth, followed by stabilisation. In contrast, the results at pH 10 and 11 show slower growth.

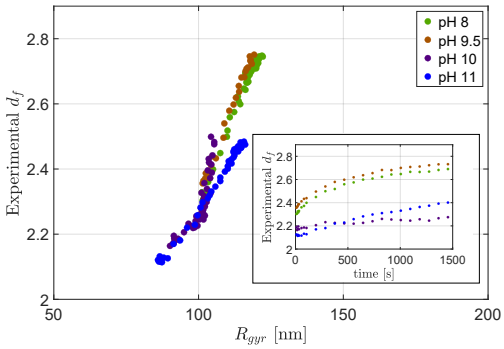

Figure 3: Experimental SAXS data acquired following the agglomeration process of a boehmite powder at 5 g/L which was brought to a pH 10 stanting from and initial pH of 3.

A similar behaviour to that of the DLS gyration radius is thus observed for the SAXS fractal dimension. This may be due to a different agglomeration mechanism in the initial instants of the process, since for all pH values, after an initial growth phase (fast or slow) the size and fractal dimension tend to stabilize.

4.2. Comparison between population balance and Brownian dynamics model

During the first instants of the agglomeration process, particles tend to form linear agglomerates, before undergoing a rearrangement that increases their fractal dimension. This is illustrated by the Brownian-DLVO simulations (Fig.4), showing the evolution of the agglomerates arrangement with time. The fractal dimension evolution with respect to the average agglomerate diameter is reported in the phase diagram obtained from the Brownian-DLVO simulations in Fig.5, in the corner it is also reported the evolution of the average fractal dimension, which increases linearly with time in the first instants and stabilizes afterwards.

It can be assumed that the fractal dimension and the gyration radius respect a relationship of the type

$$d_f = d_{f,1} + (d_{f,2} - d_{f,1}) \cdot \frac{atg\left(a_a \cdot \frac{R_{gyr} - R_{cut}}{R_{cut}}\right) + \frac{\pi}{2}}{\pi} \tag{20}$$

which can represent the two plateaus of Fig.5 by means of the following parameters

- a_a enables to vary the slope of the d_f rise

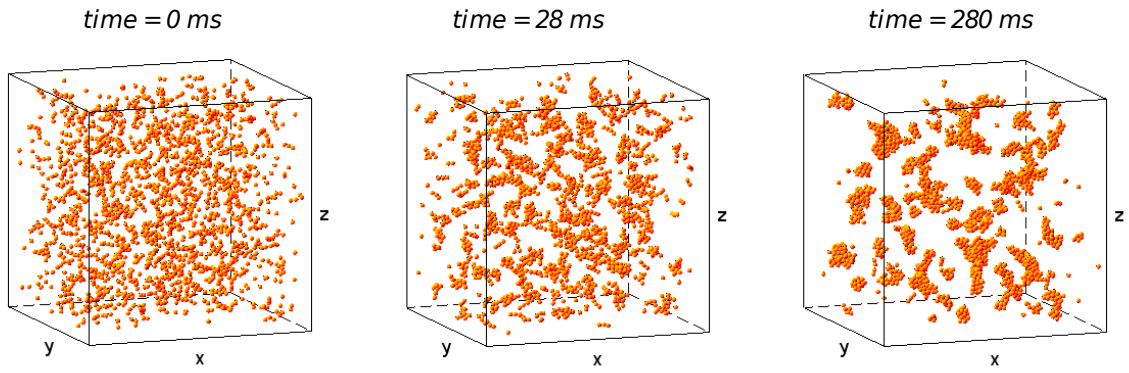

Figure 4: Configuration of the agglomerates system at different time instants, simulated with Brownian dynamics model.

- R_{cut} corresponding to the abscissa of the inflection point, is the cutoff gyration radius.
- $d_{f,1}$ and $d_{f,2}$ are two parameters that, together with a_a determine the value at the two plateaus d_{min} and d_{max}. If $a_a \geq 20$ then $d_{f,1} \simeq d_{f,min}$ and $d_{f,2} \simeq d_{f,max}$.

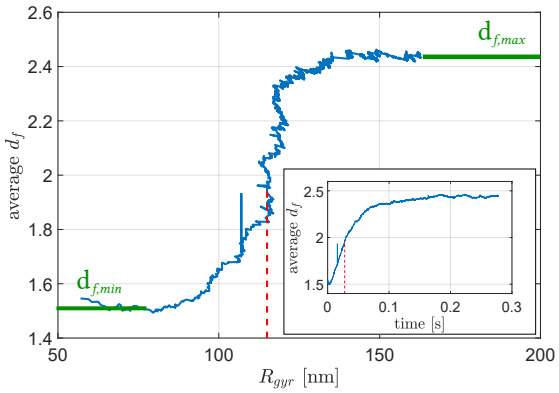

Figure 5: Illustration of the phase diagram and of the parameters of the Eq.(20). The evolution of the average fractal dimension over 0.3 s is reported in the right corner.

The fact that the fractal dimension evolves with the size of the agglomerate during agglomeration has also been observed with SAXS analysis as it is reported in Fig.3. The experimental curve cannot represent the two plateaus since the initial primary particle and the finale agglomerate are out of the measurement size limits. In addition, the non-spherical geometry of the primary particle may have an impact on the agglomerate fractal dimension, which can explain the difference between the d_f simulated by the Brownian Dynamic model and the one measured with SAXS analysis.

By fitting the phase diagram obtained from Brownian-DLVO simulations with Eq.(20) the results obtained for $d_{f,1}$ and $d_{f,2}$ are 1.53 and 2.48 respectively, a_a is 25.69 and R_{cut} is 115 nm.

These parameters has been used to model the d_f vs R_{gyr} relationship of the population-balance model. The particle size and concentration have been taken equal to the Brownian Dynamics model. In order to simulate a physical time of 0.27 s the population-balance and the Lagrangian model require respectively 10 s and 3 weeks of computational time.

Fig.6(a) shows the comparison between the evolution of the average diameter as a function of time between the Lagrangian Brownian-DLVO model and the population-balance. Fig.6(b) shows the results in terms of cluster mass distribution at the time 0.278 ms.

The two models are in fair agreement for $W = 1.7$. This value is close to 1 when the pH of the suspension is close to the Point of Zero Charge (PZC), and it is highly sensitive to small varitions of pH. Therefore the Fuchs coefficient is still in the order of magnitude estimated for these conditions. It is experimentally challenging to measure a Fuchs stability ratio and small variations are tolerable if W remains within the right order of magnitude. The population balance respects the time scale of the coagulation simulated via Brownian dynamics. The error between 0 and 0.05 s can be explained by the fact that the Lagrangian simulation accounts only for 2048 particles. Consequently the Brownian dynamics is less statistically representative of a real colloidal system.

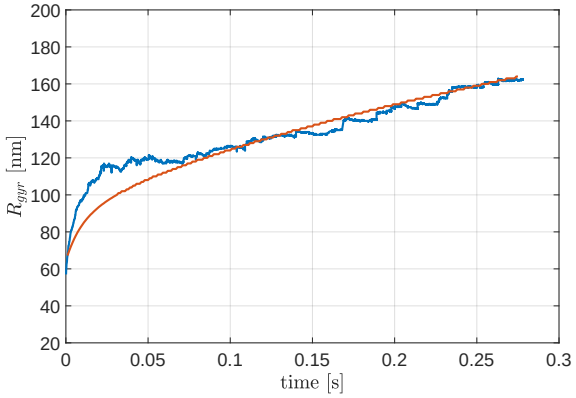

(a)

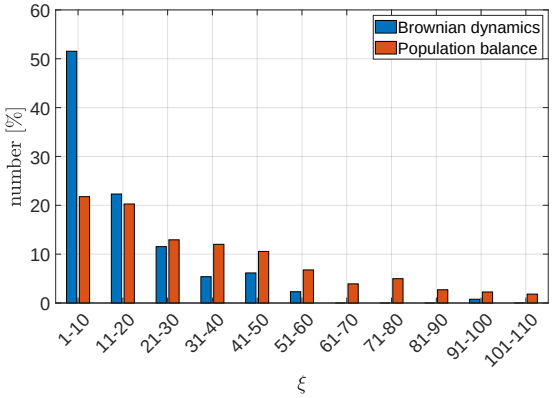

(b)

Figure 6: Comparison between the Lagrangian simulation and the population balance in terms of average diameter evolution (a) and final mass distribution (b) after 0.278 s.

4.3. Adjusting population balance parameters with DLS results

The population balance result is reported in Fig.2(a). The Tab.1 reports the parameters obtained for the different DLS experiments. All the data were compared with the population balance model using a $d_{f,1}$ of 1.5. $d_{f,2}$ and R_{cut} vary within a narrow range. The parameter that has the highest impact is the Fuchs stability ratio W_{PBE}. Indeed for the data set at pH 11, for which $W_{PBE} = 31.14$, the population balance result is independent of the values of all the other parameters. W_{PBE} appears to be between the theoretical and the experimental Fuchs stabiity ratio as shown in Fig.2(b).

The comparison between the population balance and the DLS data obtained at low boehmite concentration enables to set ranges for the parameters of the model, which make it capable to represent evolution of suspensions at higher concentration. In order to approach the boehmite concentration of the manufacturing process the population balance was extrapolated at a concentration of 1 g/L and at PZC. Fig.7(a) shows the mass cumulative distribution after an agglomeration process of 1 hour, when it is assumed that the colloidal systems has reached the equilibrium size distribution.

Table 1: Adjusted parameters of the population balance model.

pH	8.8	9.3	9.7	10.5	11
$d_{f,2}$	2.75	2.75	2.75	2.85	/
R_{cut}	600	596	607	600	/
a_a	3.96	3.97	2.69	1.8	/
W_{PBE}	1.32	1.31	1.17	2.50	31.14

This result has been used to adjust a morphological model of a powder obtained by drying the suspension.

In order to build the morphological model of a boehmite grain formed after Brownian agglomeration, the primary aggregates are considered as spheres with radius 35 nm in agreement with DLS measurement. Keeping the aim of reducing the computation time, we considered a discretized cumulative distribution (Fig.7(a)). Seven agglomerates have been built with a number of primary particles ranging from 25 to $81{\cdot}10^5$ in order to cover the entire distribution. The fractal dimension of these agglomerates is computed with the adjusted $d_f(xi)$ relationship, and it takes a value of 1.70 for the smaller agglomerates and of 2.82 for the larger ones.

In Fig.7(a) the red points represent the discrete cumulative distribution obtained assembling 100 agglomerates. The coagulation of these agglomerates has been simulated via the morphological model [8] where the maximum compactness parameters have been set. An illustration of the morphology of the final dry powder is shown in Fig.7(b).

5. Conclusion

Boehmite agglomeration phenomenon is extremely chaotic and involves assembly at multiple size scales, from a few tens of nanometers to several microns. The use of multi-technique characterizations highlights structural properties at different scales. A strategy has been developed for gener-

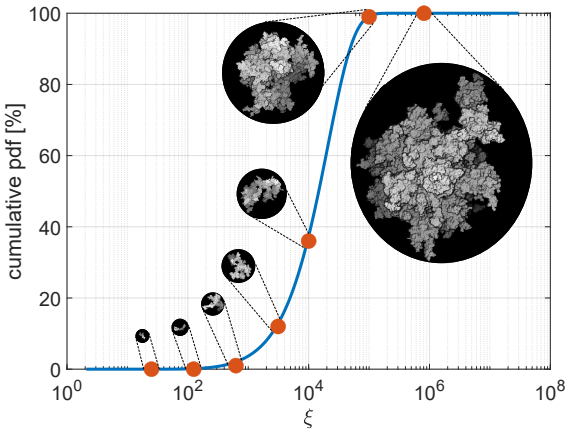

(a)

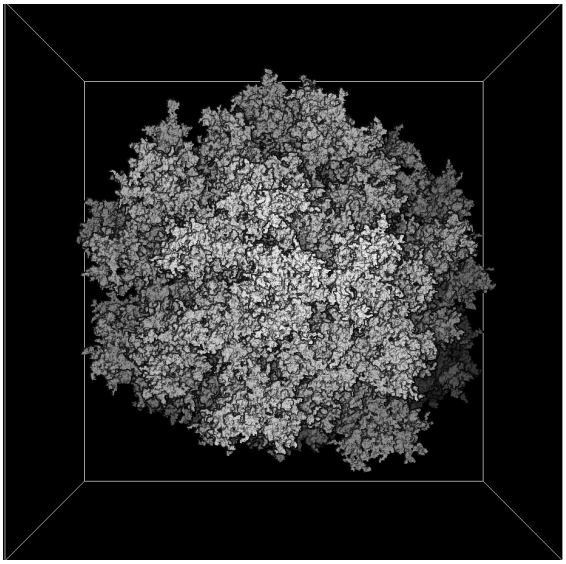

(b)

Figure 7: (a)Cumulate probability density function obtained from a population-balance simulation. The operating conditions are pH = 9.6 and 1g/L, the time simulated is of one hour. The seven agglomerates of the discrete distribution are also represented. (b)Simulated morphology of a boehmite dried powder after agglomeration within a colloidal suspension at 1 g/L ad PZC.

ating the 3D morphology of a boehmite grain after agglomeration in a colloidal suspension. Our contribution consists in describing a system that evolves according to physical-chemical parameters as a function of structural parameters like size distribution, fractal dimension and order of assembly. The final microstructure is generated with an aggregation morphological model where different sticking probabilities are assigned on concave and non-concave points of a cluster. In order to rely these probabilities to physical-chemical parameters, two physical models have been used: a Lagrangian Brownian dynamics model and a population balance model. The first one provided information about the relationship between fractal dimension and agglomerate mass ξ. The second one enables to simulate a realistically large colloidal system. Since the relationship found with the first model can also be confirmed by SAXS analysis results, the function $\xi(d_f)$ has been implemented in the Smoluchowski kernel of the population balance model. DLS experimental results have been used to adjust the kernel parameters. The size distribution and the fractal dimension obtained from the population balance was finally used to parameterize the morphological model and to build an agglomerate of agglomerates.

The experimental DLS results are qualitatively in agreement with the DLVO theory, indeed the closer the pH to the point of zero charge, the faster the agglomeration process is. The resistance to agglomeration has been quantified via the Fuchs stability coefficient. A good agreement has been found between the experimental, the theoretical and the adjusted Fuchs coefficient of the Smoluchoswki kernel.

In order to relate the morphology of an agglomerate to the conditions of agglomeration, experimental methods and models of agglomeration dynamics are often compared and inter-combined [23, 24] or a stochastic agglomeration model is parameterised using experimental data [25]. In this paper, it is proposed to use all these approaches, and in particular to use the population balance as a bridge between the experimental results and the morphological model of agglomeration.

This work has made it possible to highlight many prospects for improvement, like implementing a Brownian model with non-spherical particles, this may have an impact on the parameters of the $\xi(d_f)$ function. In addition, the natural perspective of this work is to consider boehmite crystallites as primary particles rather than aggregates. This would enable the simulation of the textural properties like pores distribution and tortuosity [26]. Then, taking into account the inclusion of shear-induced agglomeration and breakage to higher concentrations, will approach the industrial operating conditions of the manufacturing process of the support. In order to innovate catalytic materials, it would be useful to simulate the impregnation process on the modelled morphology, with the possibility of relating the ag-

glomeration pH to the dispersion of active sites on the final solid [27], and use the morphological model to feed a pore network model [28] to relate manufacturing process and textural and transport properties within a catalytic support.

Acknowledgement

DLS experiments were realized with the resources and equipment provided by IFP energies nouvelles. SAXS experiments were performed on the SWING beamline at SOLEIL Synchrotron, France. We are grateful to Thomas Bizien for assistance and to the SOLEIL staff for smoothly running the facility.

References

[1] D. Chiche, M. Digne, R. Revel, C. Chanéac, J.-P. Jolivet, Accurate determination of oxide nanoparticle size and shape based on X-ray powder pattern simulation: Application to boehmite AlOOH, The Journal of Physical Chemistry C 112 (23) (2008) 8524–8533.

[2] P. Euzen, P. Raybaud, X. Krokidis, H. Toulhoat, J. Le Loarer, J. Jolivet, C. Froidefond, Alumina, in Handbook of Porous Solids, Wiley, 2002, Ch. 4.7.2.

[3] E. J. Verwey, J. T. G. Overbeek, Theory of the stability of lyophobic colloids: the interaction of sol particles having an electric double layer, Elsevier publishing company Inc., 1948.

[4] H. Hamaker, The london-vander waals attraction between spherical particles, Physica IV 10 (1937) 1058–1072.

[5] M. V. Smoluchowski, ber brownsche molekularbewegung unter einwirkung uerer krfte und deren zusammenhang mit der verallgemeinerten diffusionsgleichung, Electrische Endosmose und Strmungsstrme (1921) 204–210.

[6] P. Langevin, Sur la thorie du mouvement brownien, Comptes-Rendus de l'Acadmie des Sciences (1908).

[7] P. C. Hiemenz, R. Rajagopalan, Principles of colloid and surface chemistry, Marcel Dekker Inc. (1986).

[8] G. Ferri, S. Humbert, M. Digne, J.-M. Schweitzer, M. Moreaud, Aggregation morphological model with variable compactness: application to colloidal system, Image Analysis and Stereology 40 (2) (2021) 71–84.

[9] R. Pecora, Dynamic light scattering: Applications of photon correlation spectroscopy, Plenum press, New York (1985).

[10] G. Beaucage, D. W. Schaefer, Structural studies of complex systems using small-angle scattering: a unified guinier/power-law approach, Journal of Non-Crystalline Solids 172 –174 (1994) 797–805.

[11] G. Volpe, G. Volpe, Simulation of a brownian particle in an optical trap, American Journal of Physics 81 (3) (2013) 224–230.

[12] P. A. Cundall, O. D. L. Strack, A discrete numerical model for granular assemblies, Gotechnique 29 (1) (1979) 47–65.

[13] W. Yang, Z. Zhou, D. Pinson, A. Yu, Periodic boundary conditions for discrete element method simulation of particle flow in cylindrical vessels, Ind. Eng. Chem. Res. 53 (19) (2014) 8245–8256.

[14] L. Gmachowski, Mass–radius relation for fractal aggregates of polydisperse particles, Colloids and Surfaces A: Physicochemical and Engineering Aspects 224 (1-3) (2003) 45–52.

[15] C. M. Sorensen, G. C. Roberts, The prefactor of fractal aggregates, Journal of Colloid and Interface Science 186 (CS964664) (1997) 447–452.

[16] A. V. Filippov, M. Zurita, D. E. Rosner, Fractal-like aggregates: Relation between morphology and physical properties, Journal of Colloid and Interface Science 229 (1) (2000) 261–273.

[17] G. Ferri, S. Humbert, J.-M. Schweitzer, M. Digne, V. Lefebvre, M. Moreaud, Mass fractal dimension from 2d-microscopy images via an aggregation model with variable compactness, Journal of Microscopy 286 (1) (2021).

[18] Y. Sun, Investigating diffusion coefficient using dynamic light scattering technique, arXiv:physics (2018).

[19] L. Pereira de Oliveira, J. J. Verstraete, M. Kolb, A monte carlo modeling methodology for the simulation of hydrotreating processes, Chemical Engineerign Journal 207–208 (2012) 94–102.

[20] H. Holthoff, S. U. Egelhaaf, M. Borkovec, P. Schurtenberger, H. Sticher, Coagulation rate measurements of colloidal particles by simultaneous static and dynamic light scattering, Langmuir 12 (1996) 5541–5549.

[21] M. Kosmulski, ph-dependent surface charging and points of zero charge. iv. update and new approach., Journal of Colloid and Interface Science 337 (2) (2009) 439–448.

[22] L. Speyer, S. Humbert, T. Bizien, V. Lecocq, A. Hugon, Peptization of boehmites with different peptization index: An electron microscopy and synchrotron small-angle x-ray scattering study, Colloids and Surfaces A: Physicochemical and Engineering Aspects 603 (2020) 125175.

[23] M. Lattuada, H. Wu, A. Hasmy, M. Morbidelli, Estimation of fractal dimension in colloidal gels., Langmuir 19 (15) (2003) 6312–6316.

[24] C. M. Sorensen, Light scattering by fractal aggregates: A review., Aerosol Science and Technology 35 (2) (2001) 648–687.

[25] E. Nakouzi, J. A. Soltis, B. A. Legg, G. Schenter, X. Zhang, T. Graham, K. M. Rosso, L. M. Anovitz, J. J. de Yoreo, J. Chun, Impact of solution chemistry and particle anisotropy on the collective dynamics of oriented aggregation, ACSnano 12 (10) (2018) 10114–10122.

[26] J. Chaniot, M. Moreaud, L. Sorbier, T. Fournel, J. Becker, Tortuosimetric operator for complex porous media characterization, Image Analysis Stereology (2019).

[27] L. Catita, E. Jolimaitre, A.-A. Quoineaud, O. Delpoux, C. Pichon, J.-M. Schweitzer, Mathematical modeling and magnetic resonance imaging experimental study of the impregnation step: A new tool to optimize the preparation of heterogeneous catalysis, Microporous and Mesoporous Materials 312 (2021) 110756.

[28] G. A. Ledezma Lopez, J. J. Verstraete, L. Sorbier, A. Glowska, D. Leinekugel-Le-Cocq, E. Jolimaitre, C. Jallut, Generation of gamma-alumina digital twins using a nitrogen porosimetry simulation, Industrial and Engineering Chemistry Research 60 (2021).

[29] D. R. E. Snoswell, J. Duan, D. Fornasiero, J. Ralston, Colloid stability and the influence of dissolved gas, The Journal of Physical Chemistry B 107 (13) (2003) 2986–2994.

Appendix A. Computation of experimental Fuchs coefficient

According to [20], the Fuchs stability coefficient can be computed at a time t close to 0 assuming that only dimers have formed at that instant. For dynamic light scattering the dimerisation kinetic constant can be approximated

$$k_{11} \simeq \frac{1}{\xi_0} \cdot \frac{R_2}{R_2 - R_1} \cdot \left(\frac{\frac{dR(t)}{dt}|_{t\to 0}}{R(0)} \right) - \left(\frac{\frac{dI(q,t)}{dt}}{I(q,0)} \right) \tag{A.1}$$

where

- R_1 and R_2 are the hydrodynamic radius of the monomer and dimer repsectively;
- $I(q,t)$ is the scattered intensity at scattering vector q and at time t;
- a is the radius of the primary particles;
- ξ_0 is the initial particle number concentration.

The stability ratio can be estimated by dividing the fast coagulation rate constant k_f by a slow coagulation rate constant k_s [29]

$$W = \frac{k_{11,fast}}{k_{11,slow}} \tag{A.2}$$

From the experimental data the average fitting curves shown have been calculated using the following functions

- from pH 8.8 to pH 10.5

$$R(t) = A \cdot log(t)^2 + B \cdot log(t) + C \tag{A.3}$$

- for pH 11

$$R(t) = D \cdot exp(E \cdot t) \tag{A.4}$$

k_{11} has been estimated with the following hypotheses:

- Since the concentration is low we assume that the contriubution of the scattered intensity is negligible with respect to the hydrodynamic radius one

$$\left(\frac{\frac{dI(q,t)}{dt}}{I(q,0)} \right) << \frac{1}{\xi_0} \cdot \frac{R_2}{R_2 - R_1} \cdot \left(\frac{\frac{dR(t)}{dt}|_{t\to 0}}{R(0)} \right). \tag{A.5}$$

Table A.2: Results of the estimation of the initial dimerization constant nd of the Fuchs stability ratio.

pH	8.8	9.3	9.7	10.5	11
$k_{11} \cdot \xi_0$	139	135	161	47	6
W_{exp}	1.16	1.19	1.00	3.45	26.75

- The lowest acquisition time with DLS device is 20 s, we assume that at this time only monomers are present. Therefore we call $R_2 = R(20s)$.

Tab.A.2 reports the results for the experiments at 0.04 g/L of Pural SB3